Combined centroid-envelope dynamics of intense, magnetically focused charged beams surrounded by conducting walls

K. Fiuza, F. B. Rizzato, and R. Pakter

Citation: Physics of Plasmas **13**, 023101 (2006); doi: 10.1063/1.2170581
View online: http://dx.doi.org/10.1063/1.2170581
View Table of Contents: http://scitation.aip.org/content/aip/journal/pop/13/2?ver=pdfcov
Published by the AIP Publishing

Combined centroid-envelope dynamics of intense, magnetically focused charged beams surrounded by conducting walls

K. Fiuza,[a] F. B. Rizzato,[b] and R. Pakter[c]
Instituto de Física, Universidade Federal do Rio Grande do Sul, Caixa Postal 15051, 91501-970, Porto Alegre, RS, Brazil

(Received 17 October 2005; accepted 9 January 2006; published online 8 February 2006)

In this paper we analyze the combined envelope-centroid dynamics of magnetically focused high-intensity charged beams surrounded by conducting walls. Similar to the case where conducting walls are absent, it is shown that the envelope and centroid dynamics decouple from each other. Mismatched envelopes still decay into equilibrium with simultaneous emittance growth, but the centroid keeps oscillating with no appreciable energy loss. Some estimates are performed to analytically obtain characteristics of halo formation seen in the full simulations. © *2006 American Institute of Physics*. [DOI: 10.1063/1.2170581]

I. INTRODUCTION

It has been established that in several situations magnetically focused beams of charged particles relax from nonstationary into stationary flows with concomitant emittance growth.[1] Such is the case of beams with an initially mismatched envelope, flowing along the magnetic symmetry axis of focusing systems. Here the initial oscillating envelope relaxes into the equilibrium solution with simultaneous emittance growth. Gluckstern[2] shows that mismatched beams induce the formation of large-scale resonant islands beyond the beam border.[3] Beam particles could be captured by the resonant islands, departing from the beam vicinity. That would cause noticeable emittance growth, along with the associated decay into equilibrium.

It is also a matter of recent interest to understand the dynamics of beams displaying some misalignment with respect to the symmetry axis of the focusing system. In a series of modern high-intensity vacuum electronic devices it is expected that off-axis beam dynamics develops as a result of small deviations between the beam injection direction and the magnetic axis.[4] This is potentially hazardous since off-axis dynamics can ultimately lead to collision between the charged beam and the conducting walls surrounding the focusing system.[4,5] Off-axis dynamics also represent a type of beam mismatch and it is of interest to learn whether or not off-axis beams can decay into equilibrium with accompanying emittance growth.

In recent papers it has been determined that for linear focusing, and in the absence of surrounding conducting walls, envelope and centroid dynamics become totally uncoupled in the sense that the relative dynamics of particles with respect to the centroid is unaware of the centroid dynamics.[6,7] Under these conditions there is no available channel along which the excess energy of a possible centroid motion could be thermalized or converted into emittance, which is ultimately associated with the rms size of the beam envelope. The fact is that one has not the needed nonlinearity to secure the coupling between the envelope and the centroid.

But, as mentioned, this is so only in the absence of conducting walls surrounding the beam. If walls are introduced so as to represent more realistic settings, we shall see that the essential feature added is the nonlinear interaction between beam particles and the centroid. The question at this point would be on the possible conversion of the energy associated with centroid dynamics into beam emittance. Previous works assume thermalization and obtain well-defined values for emittance growth.[1] However, it is not quite clear whether thermalization can be actually realized in this instance. It is true that one has a strong nonlinear interaction involving centroid and beam particles, but we shall see that one important ingredient missing here is the presence of large nonlinear resonances induced around the beam, as it occurs for mismatches envelopes.

We pursue the issue in the present paper and our analysis finally reveals the perhaps unexpected result that centroid oscillations are quite stable and do not decay into emittance augmented beams, at least for computationally observable times. We stress that this contrast between envelope and centroid mismatches seems to be closely linked with the nonlinear dynamics of beam particles under the action of those mismatches. While in the former case large resonances form around the beam, in the latter dynamical behavior is quite regular.

To perform the investigation, we shall adopt the test particle approach.[8] Centroid and envelope bulk motion shall be initially described by approximate macroscopic governing equations, and their action on particles shall be examined as if particles were passive observers. Then, if the orbit of a relatively large fraction of particles is substantially distorted from the initially assumed beam location and shape, the macroscopic state shall be expected to decay slowly. In addition, we shall focus attention on high-intensity beams for which the spatial charge distribution can be taken as homogeneous and where emittance is initially negligible. Round beams and

[a]Electronic mail: kfiuza@if.ufrgs.br
[b]Electronic mail: rizzato@if.ufrgs.br
[c]Electronic mail: pakter@if.ufrgs.br

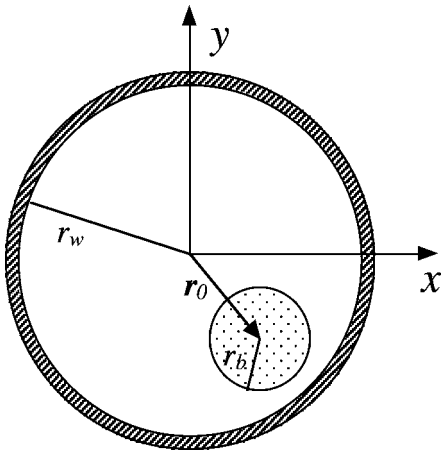

FIG. 1. Cross section geometrical aspects of the system.

solenoidal field configurations for the focusing magnetic field will be considered here.

Our paper is organized in the following form: in Sec. II we introduce the basic model as well as the macroscopic model for beam dynamics. In Sec. III we study the microscopic particle dynamics comparing the test particle approach with full self-consistent simulations. We first review and add new information to the case of purely mismatched envelopes and their corresponding resonant islands, in order to set a reference with which we compare further results. Then, the role of centroid dynamics in the problem of emittance growth is investigated. In Sec. IV we conclude the work. Full self-consistent simulations make use of the Green's function method with a varying number of particles, N, up to $N=20\,000$;[6,7] all full simulations start with round homogeneous beams (flat top beams) without emittance (cold beams) in order to represent space-charge-dominated beams.

II. THE MODEL

A. General model

Our system is formed by a beam of charged particles moving along the inner channel of a circular conducting pipe of radius r_w; the beam is focused by a constant solenoidal magnetic field. The beam centroid is allowed to swing around the symmetry axis, so even beams with a circular cross section will induce surface charges on the walls. Given the fact that as the beam swings it generates and sees an asymmetrical distribution of surface charges, one may expect a complicated beam-envelope coupling that may not be easy to deal with.

A simplified scheme of beam propagation is pictured in Fig. 1, where we represent the cross section of a circular cylindrical pipe containing a circular cylindrical beam of radius r_b centered at the centroid coordinate $\mathbf{r}_0 \equiv x_0\hat{\mathbf{x}}+y_0\hat{\mathbf{y}}$. In general terms, the motion of a charged particle in the Larmor frame of a homogeneous focusing solenoidal field is represented by the dimensionless dynamical equation for the rescaled transverse coordinate, $\mathbf{r}=(x/r_w)\hat{\mathbf{x}}+(y/r_w)\hat{\mathbf{y}}$ (centroid coordinates are normalized accordingly),

$$\mathbf{r}'' = -\mathbf{r} - \boldsymbol{\nabla}_\perp \psi + \mathbf{F}_{\text{image}}. \tag{1}$$

Note that the dimensionless pipe radius satisfies $r_w=1$. For fast particles the longitudinal velocity $v_{z,0}$ along the z axis is approximately constant, and primes denote derivatives with respect to the longitudinal scaled coordinate $s=\sigma_0^{1/2}\ z=\sigma_0^{1/2}$, $v_{z,0}t$. Here $\sigma_0=qB_z/2\gamma\beta mc^2$ is the vacuum phase advance per unit axial length; it measures the focusing strength with B_z as the external and constant solenoidal magnetic field. $\beta=v_{z,0}/c$, $\gamma=(1-\beta^2)^{-1/2}$ is the relativistic factor, q is the individual charge of the beam particles, m their mass, and c is the speed of light. Here $\psi=\psi(\mathbf{r},s)$ is the dimensionless self-field electromagnetic potential acting on each particle and generated by the beam alone, which is obtained regardless of the pipe and that can be written in terms of the electrostatic potential ϕ as $\psi=q\phi/(\gamma m\beta^2c^2r_w^2\sigma_0)$. The associated force reads as $\mathbf{F}_{\text{beam}}\equiv-\boldsymbol{\nabla}\psi$, $\mathbf{F}_{\text{image}}=\mathbf{F}_{\text{image}}(\mathbf{r},s)$ is the dimensionless force generated by the surface charges whose structure, although not yet known, may be determined by image charge considerations, as one demands that the total electric field generated by the beam alone and by the surface charges be normal to the pipe surface. Here ψ is to be derived from the Poisson equation,

$$\nabla_\perp^2\psi = -\frac{2\pi K}{N}n(\mathbf{r},s), \tag{2}$$

with $K=2Nq^2/\gamma^3m\beta^2c^2r_w^2\sigma_0$ as the beam perveance, N as the total (and constant) number of particles per axial length, and $n(\mathbf{r},s)r_w^2\rightarrow n(\mathbf{r},s)$ as the dimensionless beam density.

As the beam swings around the axis, ψ and $\mathbf{F}_{\text{image}}$ undergo complicated modifications that are unlikely to be easily cast into closed and exact analytical forms. One thing we know for sure though is that when the walls are absent, centroid and envelopes become uncoupled.[6,7] Another key information, given by Gauss' law, is that even in the presence of conducting walls, surface charges induced by circular beams perfectly centered at the symmetry axis do not act in the inner region $r<r_w$. These two facts suggest that provided the centroid oscillations are moderate, an initially circular beam approximately preserves its circular shape at least during the initial stages of the dynamics. In the Appendix we show that this assumption is accurate enough. Then, given the fact that one has a beam of known properties oscillating around the symmetry axis, we may adopt a test particle approach with which we shall examine the occurrence of a large resonant island encircling the beam. The presence of resonances allows beam particles to perform large excursions away from the beam core, which would be highly suggestive of emittance growth and thermal relaxation.

B. Modeling beam dynamics

To carry on the analysis one must thus first of all study the dynamics of round beams of radius r_b with homogeneous charge distributions, moving in the channel of a grounded circular conducting pipe of radius r_w.

Considering the commented fact that the wall might have little influence on the beam shape, we shall take the envelope equation as the governing equation for the beam radius $r_b = r_b(s)$:[8,9]

$$r_b'' = -r_b + \frac{K}{r_b} + \frac{\epsilon^2}{r_b^3}, \tag{3}$$

where the emittance $\epsilon = \epsilon(s)$ may not remain constant for mismatched beams. One feature of the envelope equation to be used later is that it remains valid even if the round beam is not homogeneous. For the space-charge-dominated beams of interest here an approximate equilibrium of Eq. (3) can be expressed in the form $r_{b,\mathrm{eq}}^2 \approx K$ at the injection coordinate $s = 0$ when $\epsilon \to 0$, which is also another result to be used later on.

The outer equipotentials of a round and axially symmetric beam are identical to the equipotentials of an equivalent beam with the same amount of charge but of radius $r_b \to 0$. This simple observation aided by image charge techniques leads us to conclude that the image charge of the original beam is a point-like, or actually a line-like charge placed at

$$\mathbf{r}_{\mathrm{im}} = \left(\frac{1}{r_0}\right)^2 \mathbf{r}_0 \tag{4}$$

and endowed with a perveance $-K$. Now, a particle arbitrarily located at a point $\mathbf{r}$ inside the pipe is submitted to a total force, as represented by Eq. (1), where, considering beam homogeneity and shape, one can write

$$-\nabla_\perp \psi \equiv \mathbf{F}_{\mathrm{beam}} = \begin{cases} K\dfrac{\mathbf{r}-\mathbf{r}_0}{r_b^2}, & \text{if } |\mathbf{r}-\mathbf{r}_0| \leqslant r_b, \\ K\dfrac{\mathbf{r}-\mathbf{r}_0}{|\mathbf{r}-\mathbf{r}_0|^2}, & \text{if } |\mathbf{r}-\mathbf{r}_0| \geqslant r_b, \end{cases} \tag{5}$$

as the direct force exerted on the particle by the beam alone. As for the image force on individual particles, one can write

$$\mathbf{F}_{\mathrm{image}}(\mathbf{r}) = K\frac{\mathbf{r}_{\mathrm{im}}-\mathbf{r}}{|\mathbf{r}-\mathbf{r}_{\mathrm{im}}|^2}, \tag{6}$$

where $\mathbf{r}_{\mathrm{im}}$ is expressed in terms of $\mathbf{r}_0$ by Eq. (4). As an intermediary result, the use of Eq. (6) enables us to evaluate the average force exerted on the beam by the image charge, $\mathbf{F}_{\mathrm{image}\to\mathrm{beam}}$:

$$\mathbf{r}_0'' + \mathbf{r}_0 = \frac{1}{N}\int_{\mathrm{beam}} n(\mathbf{r})\mathbf{F}_{\mathrm{image}}(\mathbf{r})d^2\mathbf{r} \equiv \mathbf{F}_{\mathrm{image}\to\mathrm{beam}}. \tag{7}$$

We note in passing that the total self-force $\int_{\mathrm{beam}} n(\mathbf{r})\mathbf{F}_{\mathrm{beam}}d^2\mathbf{r}$ vanishes, as required by momentum conservation, as shown for the general case in Refs. 6 and 7. The integral in Eq. (7) can be readily evaluated to yield the simple result

$$\mathbf{r}_0'' = -\mathbf{r}_0 + K\frac{\mathbf{r}_{\mathrm{im}}(\mathbf{r}_0)-\mathbf{r}_0}{|\mathbf{r}_0-\mathbf{r}_{\mathrm{im}}(\mathbf{r}_0)|^2}, \tag{8}$$

which indicates that the image force is independent of the beam transverse size, as long as the beam keeps its circular shape. This is true even if the beam is thought of as a composition of core plus halo round distributions, or, in general, as long as the distributions are axisymmetric with respect to the beam center. Alternatively, arguments based on Gauss' theorem could be invoked here: the image force on beam is equal and opposite to the virtual beam force on the image, and the latter, obtained directly by Gauss' law in axisymmetric cases, does not depend on beam size. In practical terms, the beam-image interaction is totally equivalent to the interaction of two line-like charges with total perveance, K. This fact had already been suggested in a previous paper, where the authors actually conclude that the space-charge limit of intense round beams is independent of beam size or beam distribution.[10]

Equation (8) has equilibria at $\mathbf{r}_0'' = 0$. If one writes $\mathbf{r}_0 = r_0\hat{\mathbf{r}}$, then the equilibria are located at

$$r_{0,\mathrm{eq}} = \begin{cases} \sqrt{-K+1} & \text{(unstable)}, \\ 0 & \text{(stable)}. \end{cases} \tag{9}$$

However, given the fact that from the envelope equation it follows that $K = r_{b,\mathrm{eq}}^2$ and that one must satisfy the *filling* condition $r_{0,\mathrm{eq}} + r_{b,\mathrm{eq}} < 1$, the first equilibrium of Eq. (9) cannot be attained. This precludes the direct effects of the unstable point on the centroid orbit in the present case of round beams with a stationary envelope. However, one must still investigate how individual particles are affected as the centroid moves according to Eq. (8), while the envelope dynamics is governed by Eq. (3).

III. PARTICLE DYNAMICS

A. Introductory remarks and envelope mismatches

Particle dynamics is thus to be described with the help of dimensionless equations (1) and (2) augmented by the envelope equation Eq. (3) and by the centroid equation, Eq. (8). In other words, particles shall be seen as test entities driven by the bulk motion of the entire beam. And our program here, already outlined earlier, is simple. One shall look for large-scale resonances in particle phase spaces, x, x' or y, y'. The presence of resonances shall be seen, as suggestive of a mechanism capable of extracting particles from the beam core, which would increase emittance relaxing the centroid or envelope motion. Just to make it clear what we are talking about, we first examine the more explored case of beams with mismatched envelopes but no centroid motion. Fluctuations of the beam envelope around the proper equilibrium have been recognized by Gluckstern[2] as a cause for resonances around the beam. In the presence of resonances, particles undergo an evaporation-like process along the resonances with simultaneous thermalization. In Fig. 2(a) we represent in a Poincaré plot the x, x' dynamics of a set of test particles initially placed along the x axis, whose extension slightly exceeds that of the beam (in 10%); in the inner region of the beam the dynamics is purely linear and resonances are absent. From the figure we note that large resonances perceived by those particles just outside the beam surround the core. Particles can be seen as moving away from the beam surface along the resonance manifolds. Here we use $\epsilon = 0$, $r_{b,eq} = 0.25$, and $K(\epsilon = 0) = r_{b,\mathrm{eq}}^2$ along with $r_b(s=0) = 0.5$, recording the phase coordinates whenever $r_b(s) = r_{b,\mathrm{eq}}$ with $r_b' > 0$. The full simulation of Fig. 2(b) dis-

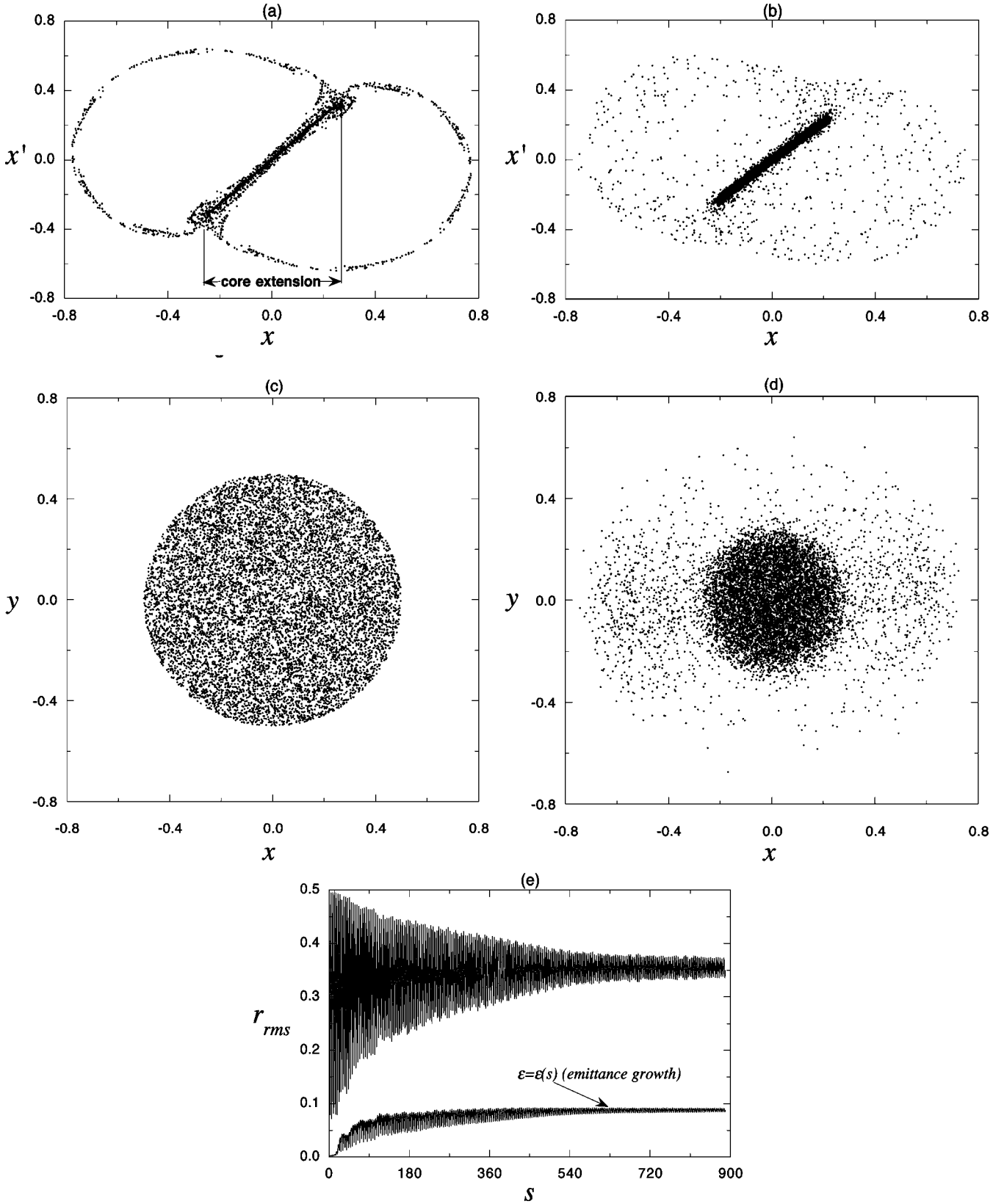

FIG. 2. (a) x,x' Poincaré plot. (b) x,x' from full simulations. (c) and (d) Initial and final x,y beam cross sections, respectively. (e) Decay of r_{rms}. In all cases here $\mathbf{r}_0=0$, $r_b(s=0)=0.5$, $K=r_b^2/4$, $\epsilon\to 0$ in Poincaré plots and $\epsilon(s=0)=0$ in full simulations.

playing the x,x' phase space of the various beam particles reveals that the low-dimensional model is fairly accurate at early times; both the Poincaré plot and full simulations run up to $s\approx 110$, which is much smaller than the relaxation time to be discussed next. As times goes on, the beam core keeps executing damped oscillations until it settles down to a value approximately corresponding to the equilibrium envelope. Meanwhile the excess energy is continuously converted into

the low-density halo until the process exhausts. Figure 2(c) represents the initial beam in a full self-consistent simulation, and Fig. 2(d) represents an asymptotic condition at $s \approx 900$, after which we do not detect substantial further changes. Panel (e) displays the rms radius

$$r_{\mathrm{rms}} \equiv \sqrt{2\langle x^2 + y^2 \rangle} \tag{10}$$

($\langle\ \rangle$ indicating an average over particles) as a function of s and indicates asymptotic damping toward $r_{\mathrm{rms}}(s \to +\infty) \equiv r^*_{\mathrm{rms}} \sim 0.353$. Also shown in panel (e) is the emittance growth obtained from full simulations; we use

$$\epsilon^2 = 4\langle x'^2 + y'^2 \rangle \langle x^2 + y^2 \rangle - \langle xx' + yy' \rangle^2. \tag{11}$$

In the final state the core occupies a region delimited by $r \lesssim r_{\mathrm{core}} \approx r_{b,\mathrm{eq}}(\epsilon = 0)$ as mentioned above and at this point the halo radius is seen to be the same as the resonance size, $r_{\mathrm{halo}} \sim 0.75$. Now a crude estimate can be made to determine r^*_{rms}. Let us first introduce what we call the magnetic energy, E_{mag} as the average canonical energy in the Larmor frame associated with the linear, or harmonic, term of Eq. (1): $E_{\mathrm{mag}} \equiv [(x^2+y^2)/2] = r^2_{\mathrm{rms}}/4$. We suppose that the excess magnetic energy per particle,

$$E_{\mathrm{mag},0} - E_{\mathrm{mag},f} = \frac{r_b^2(s=0) - r^{*2}_{\mathrm{rms}}}{4}, \tag{12}$$

which measures the corresponding difference between initial and relaxed states, decays into thermal motion

$$E_{\mathrm{kin},f} = \langle x'^2 + y'^2 \rangle = r^{*2}_{\mathrm{rms}} \epsilon, \tag{13}$$

the last equality making use of the connection between the average kinetic energy and emittance for stationary beams.[8] The electromagnetic energy of self-fields is not involved, since for large positive mismatches, $r > r_{b,\mathrm{eq}}$ it does not depend as strongly as the magnetic energy on the beam shape, provided the beam is round and homogeneous. It is true that slight changes on electromagnetic energy result from halo production, but these are also small and are not included in the estimate.

The next step is to make use of the envelope equation applied for the stationary asymptotic state,

$$r^*_{\mathrm{rms}}{}'' = 0 = -r^*_{\mathrm{rms}} + \frac{K}{r^*_{\mathrm{rms}}} + \frac{\epsilon^2}{r^{*3}_{\mathrm{rms}}}, \tag{14}$$

which allows us to express the emittance in terms of r^*_{rms}. From Eqs. (12)–(14) one readily obtains $r^*_{\mathrm{rms}} \approx 0.352$ and $\epsilon \approx 0.088$, which agrees very well with the simulations. Not only that, but if one breaks up the defining equation for the average radius, Eq. (10), into its contribution coming from the core and from the halo,

$$r^2_{\mathrm{rms}} = (1-f) r^2_{\mathrm{core}} + f r^2_{\mathrm{halo}}, \tag{15}$$

one can actually determine the fraction $f \equiv n_{\mathrm{halo}}/N$ of particle evaporated into the halo. To arrive at Eq. (15) one assumes homogeneous spatial distributions both for the high-density (core) and low-density (halo) components of the particle distribution whose x, x' projection is seen in Fig. 2(b). Under the uniformity condition, the rms and extreme radii for core and halo distributions coincide. Note that part of the halo population also occupies the core $r < r_{b,\mathrm{eq}}$, only that in this region the corresponding velocities are large.

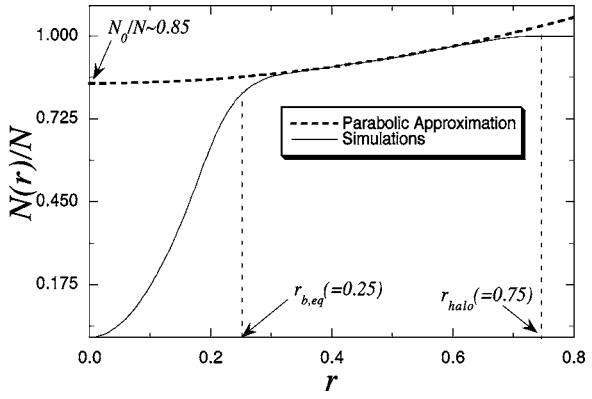

FIG. 3. Parabolic fitting to determine the halo fraction f.

For the numbers we are using here, the fraction reads as $f \approx 0.12$, again in nice agreement with the one obtained in the simulations, ~ 0.15. To determine the number of particles in the halo from the simulations, we plot $N(r)/N$ vs r from the asymptotic data of Fig. 2(e). $N(r)$ is the number of particles with a radial coordinate smaller than r. Then we fit the curve so obtained for $r > r_{\mathrm{core}}$ (beyond the core) with a parabolic shape (assuming halo density approximately constant) and find the intersection N_0/N of the parabola with $r=0$. N_0 is the number of particles in the core and the quantity $[(N-N_0)/N]$ yields an estimate of the total population within the halo. The procedure is graphically displayed in Fig. 3. The assumption on the homogeneity of the halo distribution is the simplest and is based on the tendency of space-charge-dominated beams toward uniform distributions. It is also compatible with the parabolic behavior of $N(r)$ outside the core since for constant density, $N(r) \sim r^2$. Furthermore, if one removes particles simultaneously populating the high-density central region of Fig. 2(b) and the corresponding region on the y, y' space, one shows that the population left (halo) follows a parabolic distribution also for $r < r_{b,\mathrm{eq}}$.

Figure 2(c), in fact, tells us that the halo component of the beam becomes a little distorted toward an elliptical shape as times advances. This is expected and has to do with nonlinear anisotropic instabilities (as opposed to the more well-known linear instabilities[11–13]) occurring for largely mismatched beams,[14] but does not seem to largely affect the agreement between simulations and estimates.

B. Mismatched centroids with matched envelopes

We now investigate the case where the envelope is initially set to its equilibrium value $r_{b,\mathrm{eq}}(\epsilon = 0)$ but the centroid is set to move. We take as initial conditions $\mathbf{r}'_0 = 0$ along with $\mathbf{r}_0 = 0.2\hat{\mathbf{x}}$, which is a large value for the centroid mismatch. Our intention is simply to magnify effects and determine some sort of upper bound for the action, if any, of the centroid on the relaxation processes. The centroid has zero angular momentum, and this represents a large class of settings where the beam does not rotate in the Larmor frame.

We start by depicting the relative phase coordinates $x - x_0$, $x' - x'_0$ in Fig. 4(a), the subscripted variables denoting

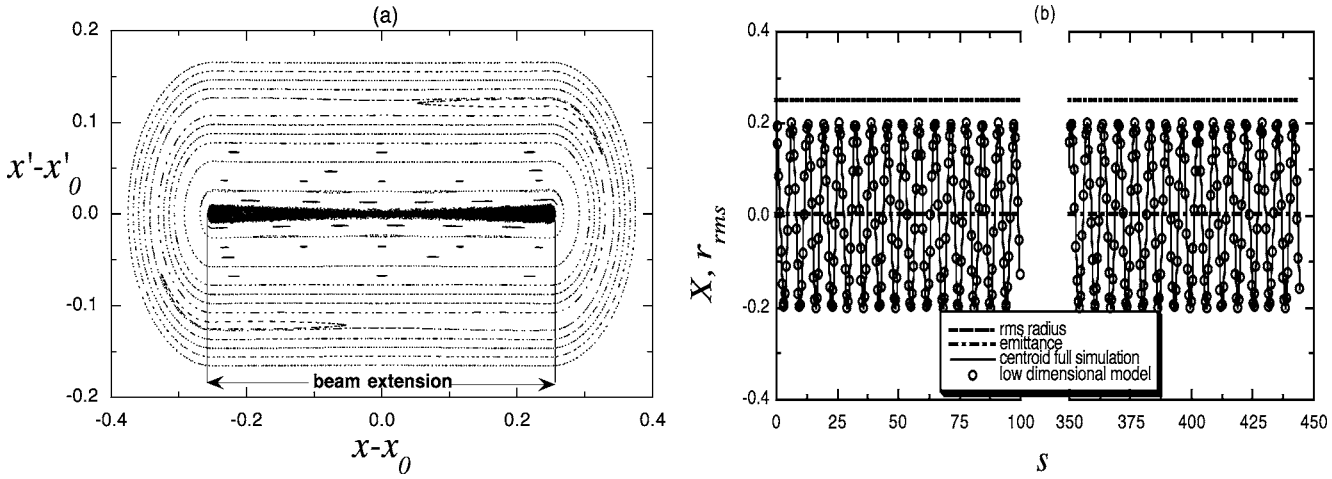

FIG. 4. (a) $x-x_0$, $x'-x_0'$ Poincaré plot. (b) $r_{\rm rms}$ and x_0 as functions of s. Here $x_0(s=0)=0.2$, $r_b(s=0)=0.25$, $K=r_b^2=0.25$. Emittances as in Fig. 2.

the position and velocity of the beam centroid, as defined earlier. We record the variables whenever $x_0=0$, $x_0'>0$; analysis of y,y' dynamics yields similar conclusions. The surprising result is that despite the nonlinear forces on the beam particles arising from the image charges, no large-scale resonance is seen in the phase plots. This fact strongly suggests that centroid oscillations simply do not find any channel along which to decay with the subsequent thermalization and emittance growth, as it occurred in the previous case. To look at this issue in some detail, consider Fig. 4(b). In the figure we plot the rms radius, now defined relative to the centroid coordinates, over a long time interval containing many centroid oscillations, which are also represented there. The centroid oscillations are obtained both from full simulations and from our low-dimensional model, Eq. (8), and we display results corresponding to the very initial and very final cycles of a relatively long computer run. As the figure reveals, quite at variance with the previous case, no changes are seen in $r_{\rm rms}$ as a function of the propagation coordinate s. Emittance, also seen in Fig. 4(b), does not grow, staying nearly zero for the entire run. As for the centroid, we note that no significant energy losses do occur for this variable as well. In particular, the agreement between full simulations and the low-dimensional model is remarkable. What one learns at this point is thus that as long as the beam envelope is matched, centroid and envelope dynamics are uncoupled, just like in the case where walls are absent.[6,7]

C. Fully mismatched beams

We are now in the position of asking what would happen if the envelope and centroid were initially injected simultaneously away from their respective equilibrium, or matched, values. As suggested by the previous case of matched envelopes, we may expect a negligible effect coming from the image charge forces acting on a beam particle. Again, this follows from the fact that centroid dynamics does not perturb the dynamics of particles far from the beam. To make sure that this is what happens we initially represent in Fig. 5(a) the x,x' surface-of-section phase space of an initially mismatched beam with $r_b=0.5$, $r_{b,\rm eq}(\epsilon=0)=0.25$ and $\mathbf{r}_0=0.2\hat{\mathbf{x}}$, $\mathbf{r}_0'=0$. Once again, just like in Sec. III A we record at $r_b=r_{b,\rm eq}$ and $r_b'>0$ the relative phase coordinates $x-x_0$ and $x'-x_0'$. What is seen is that the halo is again shaped according to the envelope nonlinear resonances alone, similar to the case analyzed in Sec. III A. The resonances sizes arising from the envelope dynamics alone are still determining to what extent a particle can move off the beam. Since these off-beam excursions are what essentially induces emittance growth, we are then inclined to conclude that even for fully mismatched beams, emittance growth is still essentially governed by the envelope mismatch.

Our last goal in this paper is thus to check the validity of these last comments. In Fig. 5(b) we depict from full simulations the decay of radial oscillations when walls are activated, for the same parameters and initial conditions used in the Poincaré plot of Fig. 5(a). As the figure reveals, the decay is similar to the one previously studied in the context of centered beams with mismatched envelopes, as represented in Fig. 2(e). In the inset we explicitly display the agreement of rms radial oscillations for both cases, at large values of s. Emittance growth exhibits the very same sort of strong similarity with the one of Fig. 2(e). Figure 5(c) shows the emittance growth for the fully mismatched beam and the inset once again reveals how similar is this present case to the one of fixed centroid as represented by the emittance growth curve seen in Fig. 2(e). Figure 5(d) finally displays the stable oscillations of the centroid. This last panel (d) also reveals once again how good is the agreement between full simulations and calculations based on the low-dimensional model, Eq. (8). The conclusion is that the coupling of the centroid and envelope dynamics is absent in the present case of beams surrounded by conducting walls, similar to what happens when walls are not present.[6,7] It should be remarked that while the beam preserves axisymmetry with respect to its own center, it cannot exchange energy with the centroid motion, since under this symmetry condition the centroid is unaware of the beam size; Eq. (8). This feature would indeed suppress centroid damping or growth, in agreement with the present results, which indicate axisymmetric beam distortions.

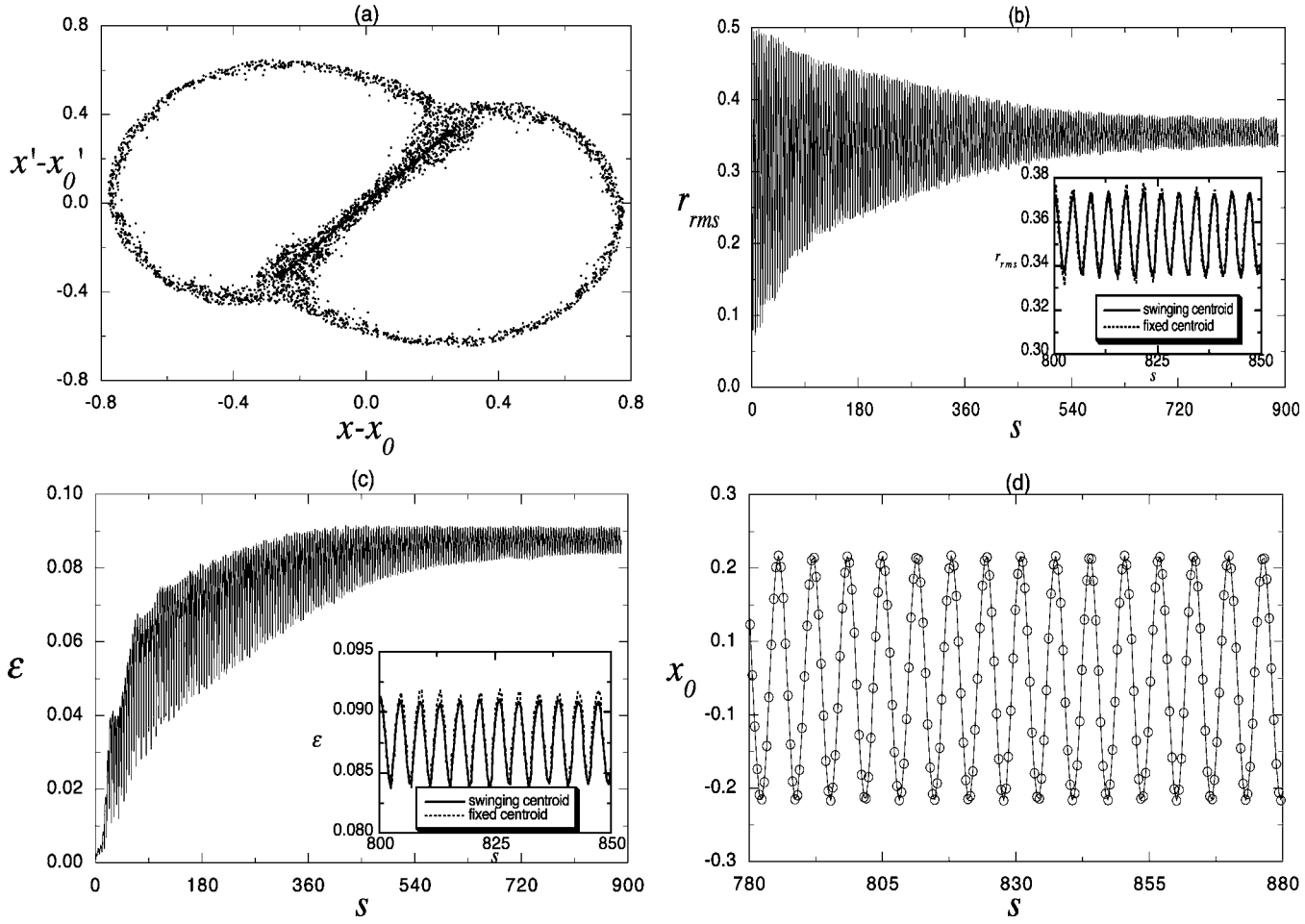

FIG. 5. (a) $x-x_0$, $x'-x_0'$ Poincaré plot. (b) Decay of r_{rms}. (c) Emittance growth. (d) x_0 as a function of s: simulations represented by circles and the low-dimensional model, Eq. (8), by the solid line. $x_0(s=0)=0.2$, $r_b(s=0)=0.5$, $K=r_b^2/4=0.25^2$. Emittances as in Fig. 2.

A final word should be said about the limits of the present analysis. As the beam particles approach the wall, the beam tends to become a little distorted and one might perhaps expect to see some collective instabilities within the beam body. This is the precise situation represented in Fig. 5, where $\{x_0\}_{\max}+r_h\approx 0.2+0.75=0.95\sim 1.0=r_w$. However, even under such extreme conditions, test particle models still agree with full simulations, as can be seen from panel (d) of Fig. 5. Other regimes have been tested like that of higher centroid mismatches combined with matched envelopes, $\{x_0\}_{\max}+r_{b,\mathrm{eq}}=0.7+0.25=0.95$, and agreement is still excellent. This in fact indicates the absence of important collective instabilities. As for centroid instabilities they have already been ruled out as a result of condition (9) along with the accompanying comments.

IV. CONCLUSIONS

In the present paper we analyze the combined envelope and centroid dynamics of magnetically focused intense charged beams surrounded by conducting cylindrical walls. Even for the extreme cases investigated, no coupling involving these macroscopic quantities has been noticed.

In particular, when the envelope is initially set at its matched equilibrium value, it stays there no matter how large might be the mismatched centroid excursions. This means that the centroid dynamics cannot decay, delivering its excess energy to internal energy of the beam, which would cause thermalization and emittance growth. Once the centroid is set to swing around the symmetry axis, it keeps its oscillatory motion at least within the computational time scales of our runs. Complementarily, if the envelope and centroid are both initially mismatched, the envelope dynamics decays toward its matched equilibrium, exhibiting emittance growth and other typical features like halo production, but the centroid simply keeps oscillating again.

The present results extend the previous investigation on the coupling of envelope and centroid dynamics in the absence of surrounding walls.[6,7] In these previous works it has been possible to show formally the uncoupled nature of the combined dynamics. Here we make use of analytical estimates as well as Poincaré plots and full simulations to conclude likewise.

Although a good deal of research may be necessary along the lines presented in the paper, it seems possible to look at some implications of the present findings. Once one is able to inject beams with matched envelopes, the centroid can be set to relatively large excursions without incurring

into the danger of beam losses via emittance growth. That might be useful in the design of oscillating devices in vacuum electronics.

ACKNOWLEDGMENTS

We acknowledge financial support from the Brazilian agencies CNPq, CAPES, and FAPERGS. We are also indebted to Wilson Simeoni, Jr. for fruitful discussions on emittance growth.

APPENDIX: BEAM SHAPE DISTORTIONS DUE TO CHARGE INDUCED AT THE CONDUCTING WALL

We consider a space-charge-dominated beam with a nearly matched radius $r_b \approx r_{b,\mathrm{eq}}$ and a centroid that swings around the system symmetry axis along a given transverse axis in the Larmor frame, namely, the x axis, such that $\mathbf{r}_0 = x_0(s)\hat{\mathbf{x}}$. In this case the beam image charge due to the conducting wall is also located at the x axis with $x_{\mathrm{im}} = 1/x_0$ (assuming a dimensionless pipe radius $r_w = 1$). Because the image charge has an opposite sign, it attracts beam particles, forcing them vertically toward the x axis and horizontally toward x_{im}. As a consequence, the beam is distorted, flattening along the y axis and stretching along the x axis in a sort of tidal effect, since the force is stronger for particles closer to the wall.

To estimate the magnitude of the beam envelope distortions, we take into consideration a cold-fluid description of the space-charge-dominated beam. The normalized steady-state cold-fluid equations for stationary flow are[8,15]

$$\frac{\partial n}{\partial s} + \boldsymbol{\nabla}_\perp \cdot (n\mathbf{v}_\perp) = 0, \tag{A1}$$

$$\frac{\partial \mathbf{v}_\perp}{\partial s} + (\mathbf{v}_\perp \cdot \boldsymbol{\nabla}_\perp)\mathbf{v}_\perp = -\mathbf{r} - \boldsymbol{\nabla}_\perp \psi + \mathbf{F}_{\mathrm{image}}, \tag{A2}$$

in accordance with Eq. (1), where ψ solves the Poisson equation (2). If we assume that the beam particles do not extend too far from the symmetry axis, such that $x_0 x \ll 1$ and $x_0 y \ll 1$ the force due to the image of the beam in Eq. (6) is approximated to first order by

$$\mathbf{F}_{\mathrm{image}} = K x_0 [(1 + x_0 x)\hat{\mathbf{x}} - x_0 y \hat{\mathbf{y}}]. \tag{A3}$$

Taking into account the way the beam is distorted by the image effects, as discussed above, we seek a solution for Eqs. (A1) and (A2) that corresponds to an elliptical beam centered at $(x,y) = (x_0, 0)$, i.e.,

$$n(\mathbf{r},s) = \begin{cases} N/\pi ab, & \text{if } \dfrac{(x-x_0)^2}{a^2} + \dfrac{y^2}{b^2} \leqslant 1, \\ 0, & \text{if } \dfrac{(x-x_0)^2}{a^2} + \dfrac{y^2}{b^2} > 1, \end{cases} \tag{A4}$$

where $a(s)$ and $b(s)$ are the semiaxes of the ellipsis. Solving the Poisson equation (2), one obtains

$$\psi(\mathbf{r},s) = \frac{K}{a+b}\left(\frac{(x-x_0)^2}{a} + \frac{y^2}{b}\right), \tag{A5}$$

in the beam interior. The continuity equation (A1) is automatically solved for a flow velocity of the form

$$\mathbf{v}_\perp(\mathbf{r},s) = \left(x_0' + \frac{a'}{a}(x - x_0)\right)\hat{\mathbf{x}} + \frac{b'}{b} y \hat{\mathbf{y}}. \tag{A6}$$

Using these results in the force, Eq. (A2), and collecting like powers of x and y, we obtain that the beam centroid and envelopes evolve according to

$$x_0'' = -x_0 + K x_0 (1 + x_0^2), \tag{A7}$$

$$a'' = -a + \frac{2K}{a+b} + K x_0^2 a, \tag{A8}$$

$$b'' = -b + \frac{2K}{a+b} - K x_0^2 b. \tag{A9}$$

Equation (A7) is equivalent to the centroid equation (8) valid for small x_0 up to cubic terms. Equations (A8) and (A9) show that because of the image effects, a nearly matched beam with $r_b \approx r_{b,\mathrm{eq}} = K^{1/2}$ will start developing small ellipticity with semiaxis a and b oscillating around the unperturbed *equilibrium* values $a_{\mathrm{eq}} = b_{\mathrm{eq}} = r_{b,\mathrm{eq}}$. In terms of order of magnitude,

$$a \approx r_{b,\mathrm{eq}}(1 + r_{b,\mathrm{eq}}^2 x_0^2), \tag{A10}$$

$$b \approx r_{b,\mathrm{eq}}(1 - r_{b,\mathrm{eq}}^2 x_0^2). \tag{A11}$$

Since $r_{b,\mathrm{eq}} x_0 \sim x x_0 \ll 1$, we see that the beam envelope distortions—proportional to $(r_{b,\mathrm{eq}} x_0)^2$—are indeed very small.

[1] A. Cuchetti, M. Reiser, and T. Wangler, in *Proceedings of the 1991 Particle Accelerator Conference*, 1991, Vol. 251; M. Reiser, J. Appl. Phys. **70**, 1919 (1991).
[2] R. L. Gluckstern, Phys. Rev. Lett. **73**, 1247 (1994).
[3] A. J. Lichtenberg and M. A. Lieberman, *Regular and Stochastic Motion* (Springer, New York, 1992).
[4] M. Hess and C. Chen, Phys. Plasmas **7**, 5206 (2000).
[5] M. Hess and C. Chen, Phys. Lett. A **295**, 305 (2002).
[6] J. S. Moraes, R. Pakter, and F. B. Rizzato, Phys. Rev. Lett. **93**, 244801 (2004).
[7] J. S. Moraes, R. Pakter, and F. B. Rizzato, Phys. Plasmas **12**, 023104 (2005).
[8] R. C. Davidson and H. Qin, *Physics of Intense Charged Particle Beams in High Energy Accelerators* (World Scientific, Singapore, 2001).
[9] P. M. Lapostolle, IEEE Trans. Nucl. Sci. **NS-18**, 1101 (1971); F. J. Sacherer, IEEE Trans. Nucl. Sci. **NS-18**, 1105 (1971).
[10] M. Hess and C. Chen, Phys. Rev. ST Accel. Beams **7**, 092002 (2004).
[11] I. Hofmann, L. J. Laslett, L. Smith, and I. Haber, Part. Accel. **13**, 145 (1983).
[12] C. J. Struckmeier and M. Reiser, Part. Accel. **14**, 227 (1984).
[13] S. M. Lund and B. Bukh, Phys. Rev. ST Accel. Beams **7**, 024801 (2004).
[14] W. Simeoni Jr., F. B. Rizzato, and R. Pakter, "Nonlinear stability of breathing beams in magnetic focusing fields" (to be published).
[15] R. Pakter and C. Chen, Phys. Rev. E **62**, 2789 (2000).